AGU PUBLICATIONS

Geophysical Research Letters

RESEARCH LETTER
10.1002/2015GL066171

Key Points:
- Different SST precursors do not favor different event types
- Thermocline depth precursors differ for EP and CP events
- Initial thermocline conditions influence the selection of the event type

Correspondence to:
A. Capotondi,
Antonietta.Capotondi@noaa.gov

Citation:
Capotondi, A., and P. D. Sardeshmukh (2015), Optimal precursors of different types of ENSO events, *Geophys. Res. Lett.*, *42*, 9952–9960, doi:10.1002/2015GL066171.

Received 11 SEP 2015
Accepted 23 OCT 2015
Accepted article online 9 NOV 2015
Published online 19 NOV 2015

Optimal precursors of different types of ENSO events

Antonietta Capotondi[1,2] and Prashant D. Sardeshmukh[1,2]

[1]CIRES, University of Colorado Boulder, Boulder, Colorado, USA, [2]Physical Sciences Division, NOAA Earth System Laboratory, Boulder, Colorado, USA

Abstract Not all El Niño–Southern Oscillation (ENSO) events are the same. Their global impacts can differ substantially depending on whether the associated sea surface temperature (SST) anomalies are stronger in the central Pacific (CP) or the eastern Pacific (EP). The predictability of such differences is therefore of interest. In this study, the optimal two-season precursors of different ENSO types are investigated in a linear inverse modeling framework using observational SST and thermocline depth data for 1958–2007. It is shown that different SST precursor types alone do not favor the generation of different ENSO types. However, initial subsurface conditions characterized by a deeper thermocline in the eastern Pacific and a shallower thermocline in the central Pacific favor the generation of EP-type events, while a shallower thermocline in the east and a deeper thermocline in the central/western Pacific are conducive to CP-type events. The predictability of different ENSO types thus depends importantly on initial subsurface conditions.

1. Introduction

The El Niño–Southern Oscillation (ENSO) is the leading mode of tropical Pacific interannual variability, with large global impacts [*McPhaden et al*., 2006]. ENSO affects ecosystems, agriculture, freshwater supplies, hurricanes, and other severe weather events worldwide. Understanding ENSO predictability is therefore an issue of high societal relevance. While the composite view of a "canonical" or generic El Niño presented by *Rasmusson and Carpenter* [1982] provided an important point of reference, individual ENSO events differ substantially in triggers, amplitudes, spatial patterns, and time evolution. The diversity in spatial pattern has become particularly noticeable in recent decades, with an apparent increased tendency to peak in the central Pacific instead of the eastern Pacific [*Lee and McPhaden*, 2010]. The atmospheric response is sensitive to interevent differences, leading to local and remote impacts that depend critically on the details of the sea surface temperature (SST) anomaly patterns, as reviewed by *Capotondi et al*. [2015].

Recent studies [*Anderson*, 2003; *Vimont et al*., 2001, 2003] have linked the onset of ENSO events to fluctuations in the amplitude of the subtropical lobe of the North Pacific Oscillation (NPO) pattern, which is the second leading pattern of wintertime sea level pressure (SLP) variability over the North Pacific [*Rogers*, 1981; *Linkin and Nigam*, 2008]. This extratropical influence may occur through the "seasonal footprinting mechanism" [*Vimont et al*., 2001, 2003] whereby atmospheric fluctuations create an SST anomaly "footprint" in spring, which persists through summer, and sustain SLP and wind stress anomalies that are conducive to the initiation of ENSO events. It may also occur through the Pacific Meridional Mode (PMM), whereby NPO-induced modulation of the trade winds leads to SST anomalies that propagate southwestward via a wind-evaporation-SST feedback mechanism [*Xie*, 1999] and promote the initiation of an ENSO event as they reach the equator [*Chiang and Vimont*, 2004; *Chang et al*., 2007]. The initial oceanic state, whether "recharged" or "discharged" in terms of the upper tropical oceanic heat content, apparently influences the PMM's efficiency in triggering ENSO events [*Anderson*, 2007; *Deser et al*., 2012]. While most studies have focused on the SST signature of the PMM, the wind stress curl anomalies associated with it can also force subsurface temperature anomalies on the equator through meridional advection. The oceanic heat content anomalies resulting from this "trade wind charging" mechanism can subsequently favor the development of an ENSO event [*Anderson et al*., 2013; *Anderson and Perez*, 2015]. In addition to the PMM, whose centers of action are in the east central subtropical North Pacific, winter SST anomalies in the northwestern subtropical Pacific (122°–132°E, 18°–28°N) have also been linked to the development of ENSO events in the following winter [Western North Pacific (WNP) precursor, *Wang et al*., 2012].

A pattern similar to the PMM also exists in the Southern Hemisphere and has been termed the South Pacific Meridional Mode (SPMM) by *Zhang et al*. [2014]. In contrast to the PMM, which has been claimed to play a key role in the generation of CP type of events [*Yu et al*., 2010; *Yu and Kim*, 2011; *Kim et al*., 2012; *Vimont et al*., 2014], the SPMM has been linked to events with the largest SST anomalies in the eastern Pacific [*Zhang et al*., 2014].

Thus, several SST and subsurface temperature precursors of ENSO events have been identified, but their relative role in triggering different event types remains unclear. Our aim here is to clarify this issue by determining the optimal two-season precursors of CP versus EP types of ENSO events using linear inverse models (LIMs) [*Penland and Sardeshmukh*, 1995; *Newman et al*., 2009, 2011] of tropical SST and thermocline depth evolution. Given the lack of consensus on the precise definition of EP versus CP events, (see *Capotondi et al*. [2015] for a review), we use the terms "CP" and "EP" loosely here to characterize events with relatively larger anomalies in the central versus the eastern tropical Pacific. We focus on two questions: (1) Can SST precursors alone help us anticipate EP versus CP warming? and (2) what is the relative importance of the surface (SST) versus subsurface (thermocline depth) precursors of ENSO diversity? We address these questions using the Simple Ocean Data Assimilation (SODA) version 2.0.2 [*Carton and Giese*, 2008] data set for 1958–2007 at monthly time resolution. An attractive feature of this data set is the dynamical consistency of its surface and subsurface fields. We use the depth of the 15°C isotherm (Z15) as a proxy for thermocline depth, and to focus on large-scale structures, we interpolate the SST and Z15 fields to 2° latitude × 5° longitude grids.

2. Optimal ENSO Precursors

The LIM methodology allows an objective determination of optimal initial conditions that develop into strong ENSO events and thus provides an ideal framework for investigating precursors. In this framework, the evolution of monthly averaged SST and thermocline depth anomalies is approximated as a linearly damped and stochastically perturbed evolution of the form

$$d\mathbf{x} = \mathbf{L}\,\mathbf{x}\,dt + \mathbf{S}\mathbf{r}\sqrt{dt}, \tag{1}$$

in which the change of the anomaly state vector $\mathbf{x}$ over a short time interval dt occurs through both deterministic processes (first term on the right-hand side (RHS) of (1)) and stochastic perturbations (second term on the RHS of (1)). The matrix $\mathbf{L}$ encapsulates the predictable dynamics of the system, $\mathbf{S}$ is a covariance matrix of stochastic perturbation amplitudes, and $\mathbf{r}$ is a random noise vector each of whose components is drawn from a normal distribution with zero mean and unit standard deviation. To isolate the relative contribution of the surface and subsurface fields, we consider two different choices for the state vector $\mathbf{x}$: in effect, two LIMs. In the first LIM, only SST components are included in $\mathbf{x}$, whereas in the second LIM, which we refer to as the extended LIM, both SST and Z15 components are included.

The data were smoothed with a 3 month running mean prior to removing the average annual cycle. Each field was then normalized by the square root of its domain-averaged variance and projected onto its leading empirical orthogonal functions (EOFs). We retained 20 SSTs and 10 Z15 EOFs, explaining 86% and 65% of the SST and Z15 variances, respectively. The components of the state vector $\mathbf{x}$ in (1) were defined as the amplitude coefficients of these EOFs. The two leading SST EOFs are shown in Figure 1. The first SST EOF (Figure 1a) shows a canonical ENSO pattern, with the largest anomalies located in the Niño 3 region, that extends toward and slightly past the dateline. Anomalies of opposite sign are seen in the western Pacific. The second SST EOF (Figure 1b) shows anomalies of one sign around the dateline and of opposite sign near the South American coast, reminiscent of CP-type events.

For a system described by (1), the most probable state at time $t+\tau$ can be determined from the state at time t as

$$\mathbf{x}(t+\tau) = e^{\mathbf{L}\tau}\mathbf{x}(t) = \mathbf{G}(\tau)\mathbf{x}(t). \tag{2}$$

By "optimal precursor" we mean an initial condition that maximizes the growth γ^2 of the state vector over a specified time interval τ. Using the L2 norm, γ may be defined as the ratio of the state vector magnitudes at lag τ and at the initial time, so that

$$\gamma^2 = \frac{\mathbf{x}^T(\tau)\mathbf{x}(\tau)}{\mathbf{x}^T(0)\mathbf{x}(0)} = \frac{\mathbf{x}^T(0)\mathbf{G}^T(\tau)\mathbf{G}(\tau)\mathbf{x}(0)}{\mathbf{x}^T(0)\mathbf{x}(0)}, \tag{3}$$

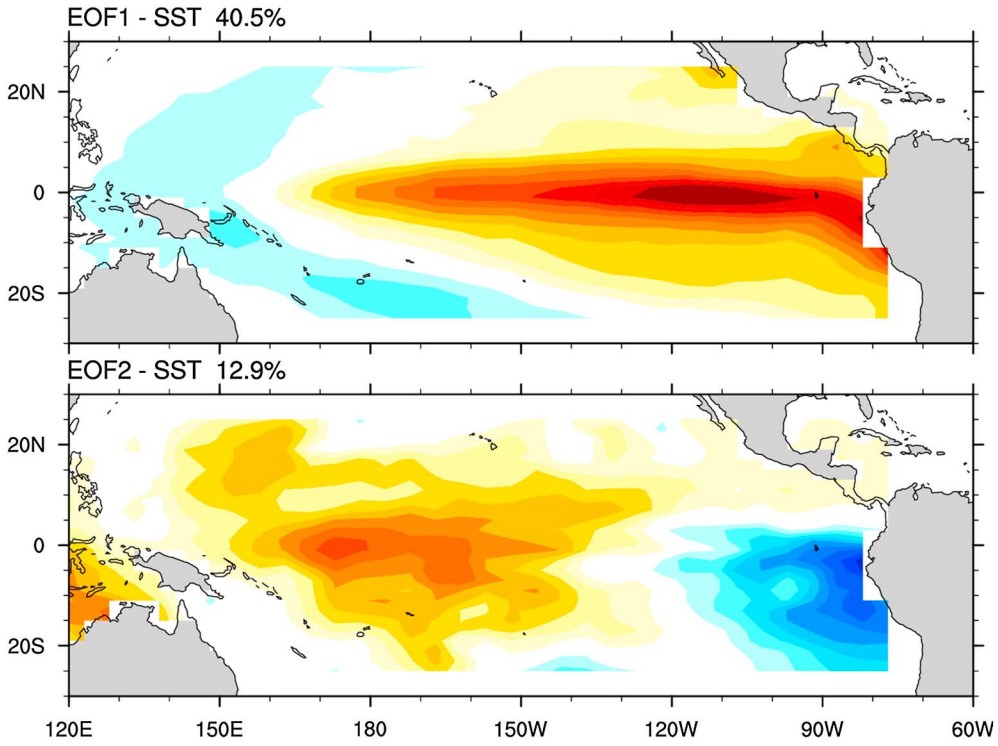

Figure 1. The two leading empirical orthogonal functions (EOFs) of monthly sea surface temperature (SST) variability in the SODA reanalysis data set for 1958–2007. Each EOF pattern is normalized to unit amplitude over the domain. Positive values are indicated by red and negative values by blue shading. (top) EOF1 accounts for 40.5% and (bottom) EOF2 for 12.9% of the total variance of the monthly SST anomalies.

where the superscript "T" indicates transpose. The optimal precursor can then be determined as the leading eigenvector of $\mathbf{G}^T(\tau)\mathbf{G}(\tau)$, which is a real, symmetric, and positive definite operator with real and positive eigenvalues $\{\gamma_i^2\}$ and orthonormal eigenvectors $\{\boldsymbol{\phi}_i\}$.

The spatial pattern of the leading eigenvector $\boldsymbol{\phi}_1$ for the SST-only LIM and $\tau = 6$ months is shown in Figure 2a. According to (2), this pattern evolves 6 months later into the optimal final structure in Figure 2d. This final structure is very similar to the canonical ENSO pattern of *Rasmusson and Carpenter* [1982]. The optimal initial

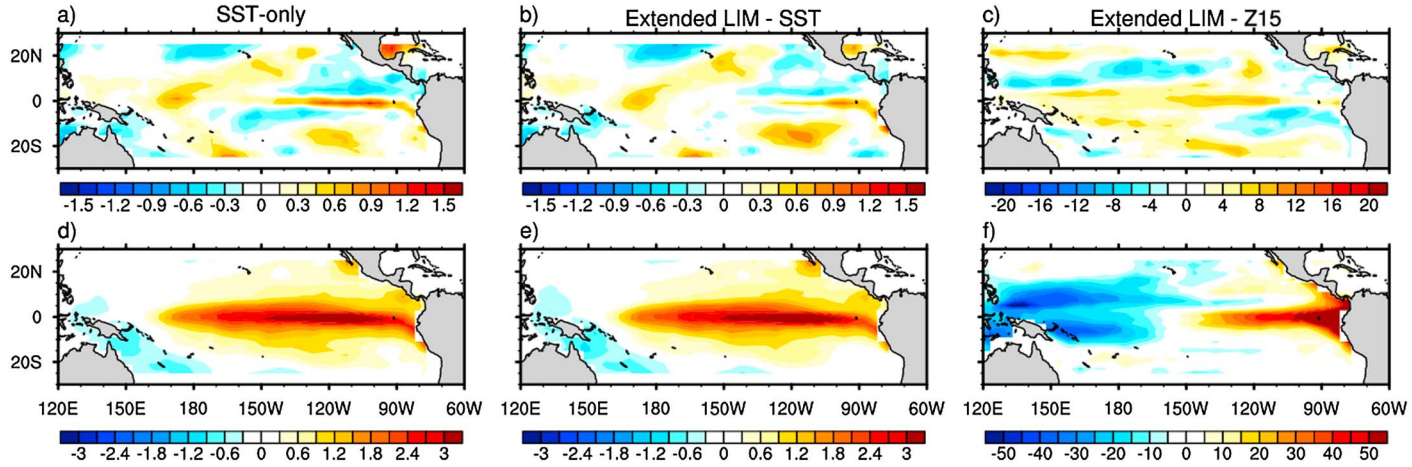

Figure 2. Optimal (a–c) initial and (d–f) final structures for maximizing anomaly growth over $\tau = 6$ months obtained using the SST-only (Figures 2a and 2d) and extended (Figures 2b, 2c, 2e, and 2f) LIMs. The optimal final patterns are obtained using a lag $\tau = 6$ months. For the extended LIM, Figures 2b and 2e show the initial and final patterns, respectively, of SST, while Figures 2c and 2f show the corresponding patterns of thermocline depth. Units are °C for SST and meters for Z15. The fields are scaled so that the final SST patterns (Figures 2d and 2e) have unit RMS values. Pattern correlation between Figures 2a and 2b is 0.88 and between Figures 2d and 2e is 0.99.

and final SST patterns determined using the extended LIM (Figures 2b and 2e) are rather similar to those in Figures 2a and 2d. However, the extended LIM provides additional information of a concurrent optimal initial thermocline state (Figure 2c) with weak positive anomalies (deeper thermocline) on the equator and weak negative anomalies off the equator, indicative of higher equatorial heat content or recharged conditions. The final thermocline pattern 6 months later is a zonal dipole structure (Figure 2f) with a deeper thermocline in the east Pacific and shallower thermocline in the west Pacific, which is characteristic of mature El Niño conditions [*Meinen and McPhaden*, 2000; *Capotondi et al*., 2006].

3. Can SST Precursors Alone Help Us Anticipate EP Versus CP Warming?

The optimal initial SST patterns in Figures 2a and 2b have several features in common with various precursors discussed in the literature. Specifically, the positive anomalies extending southwestward from Baja California to the equator are similar to the positive phase of the PMM; the negative anomalies in the northwestern corner of the domain are consistent with the WNP precursor; and the positive SST anomalies in the southeastern Pacific are reminiscent of the SPMM precursor. Do these different parts of the optimal initial anomaly pattern contribute differently to the final evolved pattern? In particular, do they contribute differently to CP versus EP warming, as suggested in some recent studies?

We address these issues in the context of the SST-only LIM, to clarify whether an initial SST anomaly pattern alone can lead to distinct ENSO types, depending on how strongly it projects on the different elements of the optimal initial SST pattern in Figure 2a. Specifically, we ask how the different parts of the optimal initial SST pattern contribute to the final mature pattern. To this end we decompose the initial vector $\boldsymbol{\phi}_1$ into four subvectors (Figure 3, left column) such that

$$\boldsymbol{\phi}_1 = \boldsymbol{\phi}_1^{(1)} + \boldsymbol{\phi}_1^{(2)} + \boldsymbol{\phi}_1^{(3)} + \boldsymbol{\phi}_1^{(4)} \tag{4}$$

and determine their contributions to the final vector, using the linear evolution equation (2), as

$$\mathbf{x}(\tau) = \mathbf{G}(\tau)\left[\boldsymbol{\phi}_1^{(1)} + \boldsymbol{\phi}_1^{(2)} + \boldsymbol{\phi}_1^{(3)} + \boldsymbol{\phi}_1^{(4)}\right]. \tag{5}$$

These different subvectors of $\boldsymbol{\phi}_1$ were first defined in physical space, in which they were spatially orthogonal by construction, and then transformed into the truncated 20 SST EOF space before evolving each of them separately using (2). Their representation in the truncated EOF basis slightly alters their structure, as seen in Figure 3 (left column) compared to Figure 2a, but each subvector still retains most of its original character. The average pattern correlation in physical space of each truncated subvector with its untruncated counterpart is 0.82, while that between each distinct pair of patterns in Figure 3 (left panels) is only 0.16. Ideally, these numbers would be 1 and 0, respectively. The contribution of each term on the RHS of equation (5) to the optimal final structure is shown in Figure 3 (right column). Remarkably, apart from slight differences in the maximum amplitude over the domain (with the weakest contribution provided by $\boldsymbol{\phi}_1^{(2)}$, the northwestern Pacific anomalies) and in the magnitudes near the South American coast, the patterns in Figure 3 (right column) are very similar to one another (average pair pattern correlation 0.92). Thus, this analysis does not support the idea that specific portions of the optimal precursor for maximizing SST anomalies in an overall sense over the domain favor warming in the central versus the eastern Pacific.

4. What Determines Central Versus Eastern Pacific Mature ENSO Anomalies?

Although ENSO events peak over a broad range of longitudes [*Capotondi et al*., 2015], our interest here is in the extreme expressions of that event distribution. One such extreme expression is events peaking in the far eastern Pacific, near the Niño 1+2 region (0°–10°S, 90°W–80°W). This class of events, which can also be identified using the *E* index of *Takahashi et al*. [2011], may include extreme cases [*Cai et al*., 2014] and is of high societal relevance to countries along the west coast of South America. We are also interested in events with positive anomalies in the central and negative anomalies in the eastern Pacific, typical of the El Niño Modoki pattern [*Ashok et al*., 2007], that have local and remote impacts differing from those of the canonical ENSO event [*Gierach et al*., 2012; *Kumar et al*., 2006; *Ashok et al*., 2007;

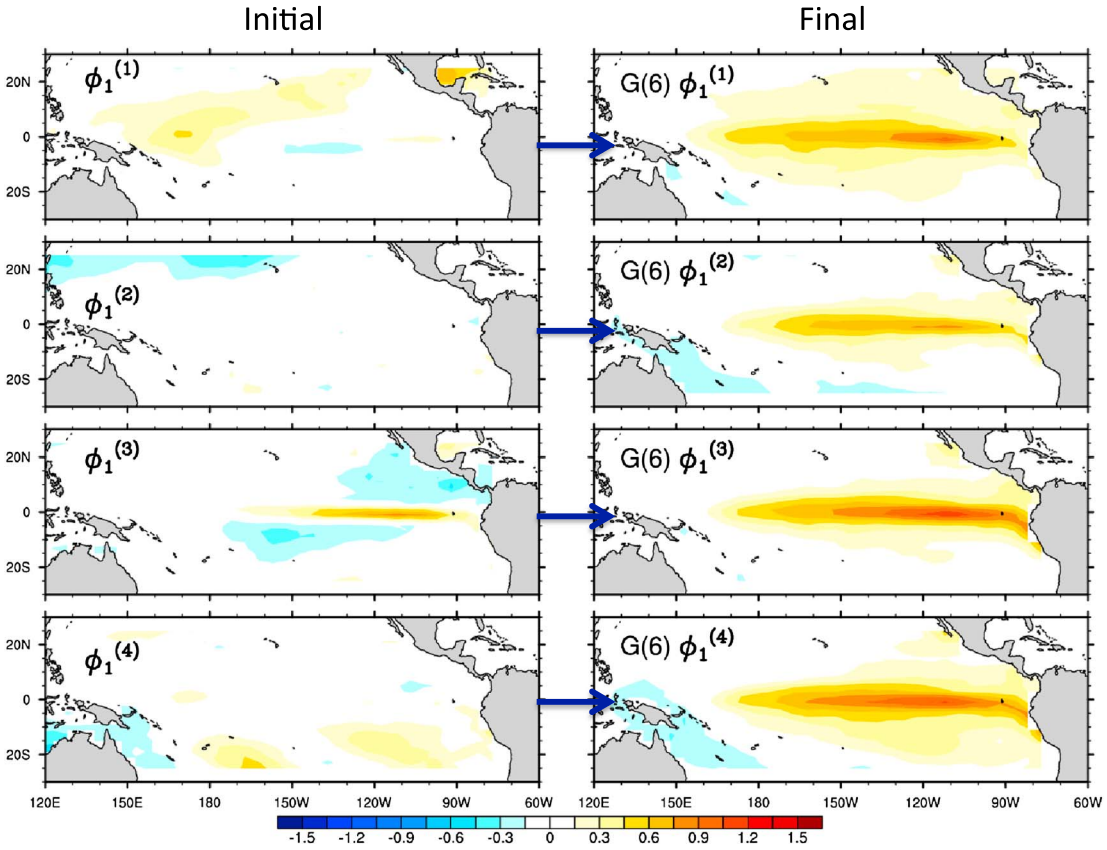

Figure 3. (left column) The decomposition of the optimal initial structure in Figure 2a into different portions, as described in equation (4). (right column) The corresponding "evolved" contribution to the final pattern in Figure 2d. The sum of the portions in Figure 3 (left column) yields the optimal initial state in Figure 2a, and the sum of the structures in Figure 3 (right column) reproduces the optimal final pattern in Figure 2d. The different portions of the optimal initial were first defined in physical space then expressed in the truncated 20 SST EOF basis for the analysis, as described in more detail in the text.

Wang and Hendon, 2007]. We identify the first class of events using the time series of the Niño 1+2 SST index and the second type using the second principal component PC2 (i.e., the amplitude time series of SST EOF2). We then seek optimal initial conditions **x**(0) that maximize the Niño 1+2 and PC2 indices at a specified later time τ (6 months). To that end, we relate each of those indices, which we will generically refer to as y, to the initial state vector as

$$y(\tau) = \mathbf{H}(\tau)\mathbf{x}(0) \tag{6}$$

and estimate **H** by linearly regressing the time series of $y\,(t+\tau)$ on the time series of **x**(t). The initial state **x**(0) in (6) that maximizes the amplitude of $y(\tau)$ with respect to $y(0)$ is then determined as the leading eigenvector of $\mathbf{H}^T\mathbf{H}$.

Figure 4a shows the optimal initial SST pattern, determined using the SST-only LIM, for maximizing the SST anomaly in the Niño 1+2 region 6 months later according to (6). There are differences with the structure shown in Figure 2a, notably the much weaker expression of the PMM, and relatively larger positive anomalies in the southeast Pacific, and along the equator east of 130°W. The evolved pattern (Figure 4d), determined using (2), has the largest SST anomalies near the South American coast, but large anomalies extend westward all the way to the dateline. The explicit inclusion of thermocline information in the extended LIM yields an optimal initial SST structure very similar to that in Figure 4a, but the final SST pattern peaks near the South American coast and remains confined to the eastern part of the basin. The optimal initial pattern of thermocline depth shows a deeper thermocline in the east and a shallower thermocline in the central/west equatorial Pacific, indicative of a reduced zonal thermocline slope and weaker upwelling in the east, a factor that can be expected to favor the development of positive SST anomalies there. Similar results are obtained when the *E* index of *Takahashi et al.* [2011] is used in (6).

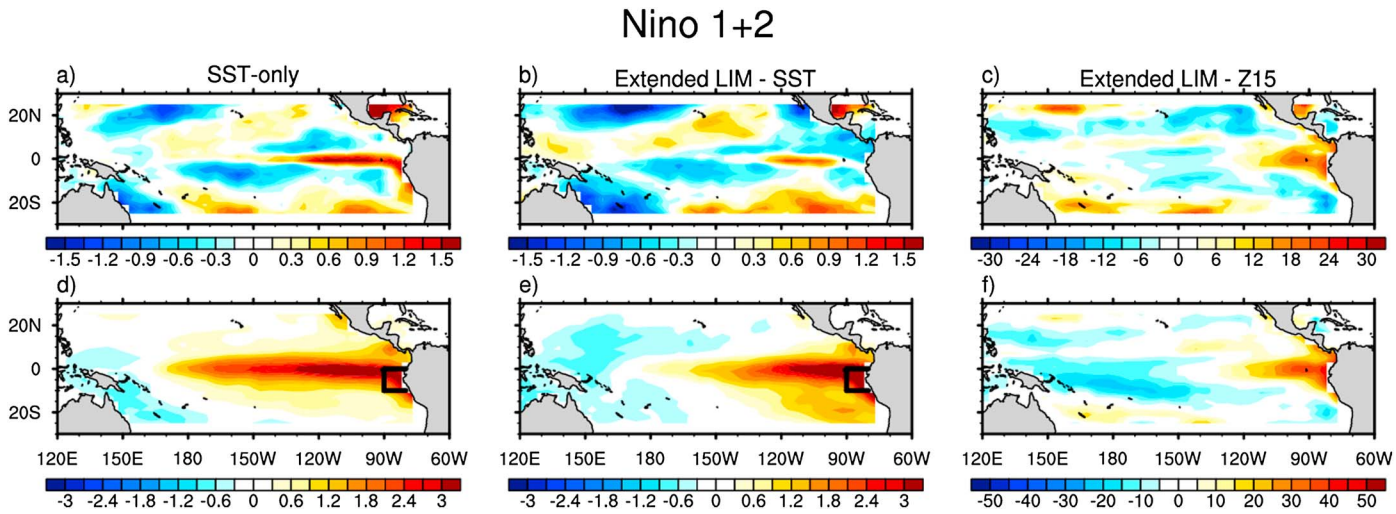

Figure 4. Optimal (a–c) initial and (d–f) final structures obtained using the SST-only (Figures 4a and 4d) and extended SST-Z15 (Figures 4b, 4c, 4e, and 4f) LIMs and equation (6), maximizing the SST anomaly in the Niño 1+2 region (indicated by the box in Figures 4d and 4e). For the extended case, Figures 4b and 4e show initial and final SST patterns and Figures 4c and 4f the initial and final Z15 patterns. For a clean comparison, the initial patterns are scaled so that the final SST fields (Figures 4d and 4e) have unit RMS values.

When maximization of EOF2 is considered, both the optimal initial (Figure 5a) and final (Figure 5d) states determined without explicit thermocline information are very similar to those shown in Figures 2a and 2d for maximizing SST anomaly magnitudes over the entire domain. Explicitly including the Z15 information results in a final SST state (Figure 5e) with positive anomalies in the central/west Pacific and negative anomalies near the South American coast, similar to the EOF2 pattern. The optimal initial state of thermocline depth anomalies in Figure 5c has a shallower equatorial thermocline in the east and deeper thermocline in the central/west Pacific, indicative of a steeper zonal thermocline slope. Our results for EOF2 are consistent with recent findings by *Mosquera-Vásquez et al.* [2013, 2014], who attribute the increased occurrence of CP-type El Niños after 2000 to the scattering of downwelling Kelvin waves by an enhanced upward thermocline slope in the eastern part of the basin. Downwelling Kelvin waves excited by anomalous westerly winds or high-frequency westerly wind bursts (WWBs) in the eastern and central Pacific have been shown to deepen the thermocline in the east Pacific and initiate the Bjerknes feedback [*McPhaden*, 1999; *McPhaden and Yu*, 1999; *Fedorov*, 2002]. However, if the altered stratification impedes wave propagation to the eastern boundary, warm anomalies may not fully develop in the eastern part of the basin and remain confined to the central part.

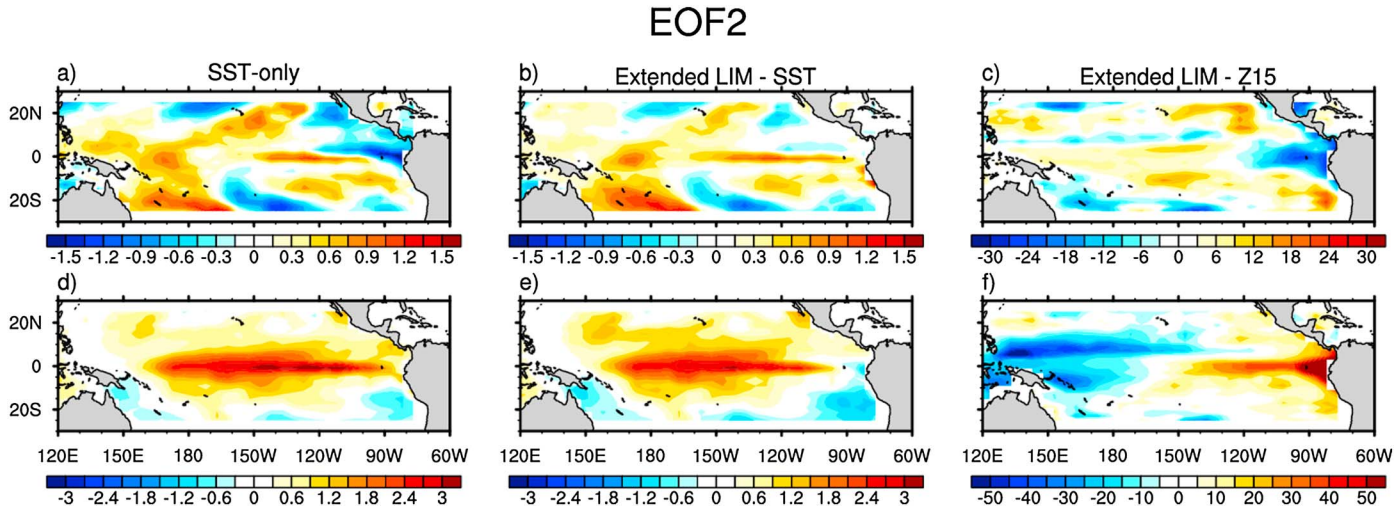

Figure 5. As in Figure 4 but for maximizing the amplitude of EOF2.

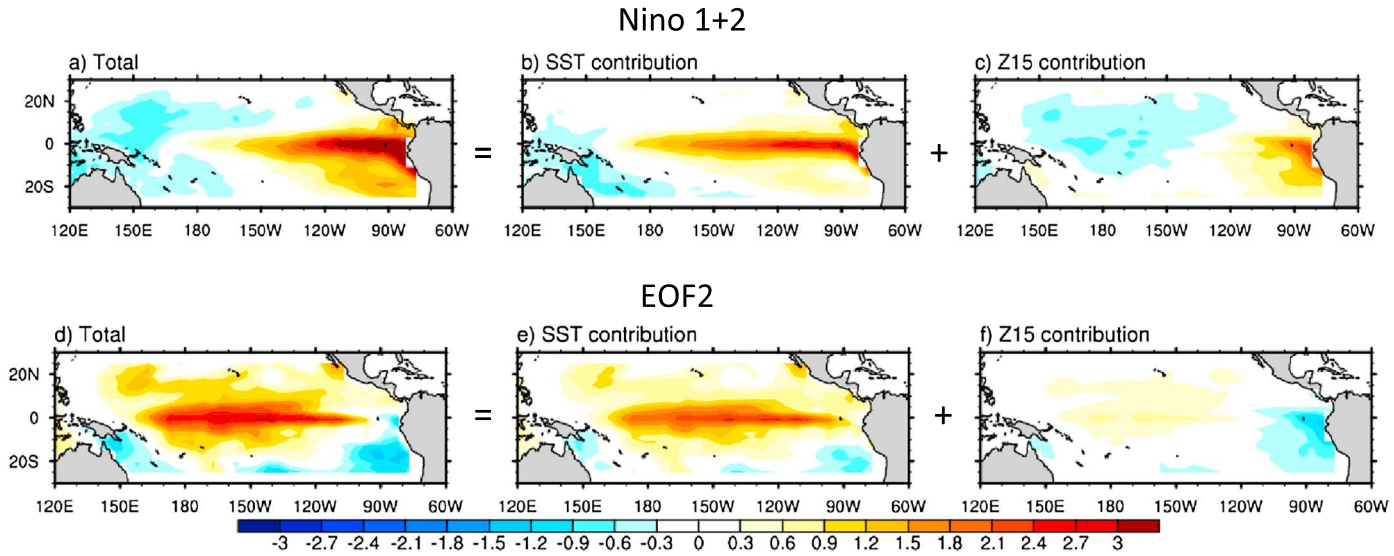

Figure 6. Contributions of the (b and e) SST and (c and f) Z15 components of the optimal initial structures to the (a and d) final evolved SST patterns in the Niño 1+2 (Figures 6a–6c) and EOF2 (Figures 6d–6f) cases. The fields have been scaled as in Figures 4 and 5. Note that the sum of the patterns in Figures 6b and 6c is equal to that in Figure 6a. Similarly, Figure 6e plus Figure 6f is equal to Figure 6d.

To further clarify the relative roles of the SST and Z15 components of the optimal initial conditions leading to the final SST patterns in Figures 4e and 5e, we separately set those components in the extended LIM to zero in (2) and examine the corresponding evolved states in Figure 6. In the Niño 1+2 case (Figures 6a–6c) the SST components of the optimal precursor lead to SST anomalies, 6 months later, extending from the far eastern Pacific to the dateline with decreasing amplitude (Figure 6b), while the Z15 components of the precursor lead to enhanced SST warming near the South American coast and weak cooling in the central Pacific (Figure 6c). In the EOF2 case (Figures 6d–6f) the steeper slope of the thermocline in the initial state contributes a weak enhancement of the central Pacific warming and cooling near the eastern boundary (Figure 6f).

5. Discussion and Conclusions

In this study we have used a linear inverse modeling approach to investigate whether specific initial SST anomaly patterns can lead to greater warmth in the central versus the eastern equatorial Pacific in the mature phase of ENSO events. Linear inverse models (LIMs) are particularly suited for investigating ENSO precursors, as they allow an objective identification of initial conditions that grow optimally into mature ENSO events. Various portions of the optimal precursor patterns thus determined by us here using the SODA data set are similar to structures previously identified in the literature as precursors of different types of ENSO events. Our results show that when only SST information is considered, these portions contribute very similarly to the final evolved mature ENSO pattern and therefore cannot help us distinguish between different ENSO types.

We find, on the other hand, that the initial thermocline state plays an important distinguishing role in the development of events peaking in the far eastern versus the central Pacific. An optimal initial thermocline that is deeper in the eastern Pacific and shallower in the central Pacific favors events peaking in the Niño 1+2 area, while a shallower thermocline in the east and deeper thermocline in the central/western equatorial Pacific leads to an SST pattern with positive anomalies in the central and negative anomalies in the far eastern part of the basin.

Previous studies [*Yu et al.*, 2010; *Yu and Kim*, 2011; *Vimont et al.*, 2014] have associated the PMM with central Pacific El Niño events. Consistent with this, the PMM portion of our optimal precursor for warming in the Niño 1+2 region (Figures 4a and 4b) is much weaker than in our canonical and EOF2 cases (Figures 2a, 2b, 5a and 5b). However, not all PMM events trigger El Niño events [*Chang et al.*, 2007], and some events peaking in the eastern Pacific, such as the strong 1997–1998 El Niño, are preceded by a positive PMM anomaly [*Larson and Kirtman*, 2014]. Our results based on the comparison between SST-only and extended LIM cases, while

consistent with findings from other researchers [e.g. *Vimont et al*., 2014], highlight the potential key role played by the initial thermocline state in the efficacy of the various precursors and in the selection of a specific ENSO type.

What might be the origin of the distinctive initial thermocline depth anomalies favoring EP versus CP warming? ENSO characteristics vary on decadal/interdecadal timescales [*Wittenberg*, 2009], and epochs dominated by EP- or CP-type events may occur as part of this intrinsic ENSO modulation [*Newman et al*., 2011]. Rectification of the ENSO signal [*Rodgers et al*., 2004; *Ogata et al*., 2013] may result in a deeper thermocline in the east and shallower thermocline in the west Pacific during EP-dominated periods, as suggested by model simulations, while the opposite may be expected during CP-dominated periods [*Choi et al*., 2012]. Indeed, observations show that the equatorial thermocline was steeper in the 2000–2010 decade (when CP events prevailed) relative to the 1980–1999 decade (when EP events prevailed) [*McPhaden et al*., 2011]. The initial thermocline conditions can also be associated with the ENSO cycle itself, and the diversity of ENSO events may arise from the interaction of stochastic atmospheric forcing (WWBs) with that cycle, as recently suggested by *Chen et al*. [2015]. Finally, a deeper thermocline in the east Pacific can arise simply from downwelling Kelvin waves triggered by WWB pulses in the early part of the year preceding the event peak.

We end by stressing that our results, and those of most other studies of ENSO precursors, are based on relatively short ~50 year records and are thus subject to sampling errors. Additional studies with multiple and longer data sets, as well as sensitivity experiments with numerical models, are needed to further elucidate the relative influence of different ENSO precursors and their robustness.

Acknowledgments

Simple Ocean Data Assimilation (SODA) data were obtained online from the SODA/TAMU research group at http://soda/tamu/edu. This study was partly supported by NOAA's Climate Program Office (CPO), DOE's Office of Science (BER), and NASA Physical Oceanography Program. The Authors thank Bruce Anderson and an anonymous reviewer for their careful reading of the manuscript and excellent constructive suggestions.

References

Anderson, B. T. (2003), Tropical Pacific sea-surface temperatures and preceding sea-level pressure anomalies in the subtropical North Pacific, *J. Geophys. Res.*, *108*(D23), 4732, doi:10.1029/2003JD003805.

Anderson, B. T. (2007), Intra-seasonal atmospheric variability in the extra-tropics and its relation to the onset of tropical Pacific sea surface temperature anomalies, *J. Clim.*, *20*, 1593–1599.

Anderson, B. T., and R. Perez (2015), ENSO and non-ENSO induced charging and discharging of the equatorial Pacific, *Clim. Dyn.*, 1–19, doi:10.1007/s00382-015-2472-x.

Anderson, B. T., R. Perez, and A. Karspeck (2013), Triggering of El Niño onset through the trade wind-induced charging of the equatorial Pacific, *Geophys. Res. Lett.*, *40*, 1212–1216, doi:10.1002/grl.50200.

Ashok, K., S. K. Behera, S. A. Rao, H. Weng, and T. Yamagata (2007), El Niño Modoki and its possible teleconnections, *J. Geophys. Res.*, *112*, C11007, doi:10.1029/2006JC003798.

Cai, W., et al. (2014), Increasing frequency of extreme El Niño events due to greenhouse warming, *Nat. Clim. Change*, *4*, 11–116, doi:10.1038/nclimate2100.

Capotondi, A., A. T. Wittenberg, and S. Masina (2006), Spatial and temporal structure of tropical Pacific interannual variability in 20th century climate simulations, *Ocean Model.*, *15*, 274–298.

Capotondi, A., et al. (2015), Understanding ENSO diversity, *Bull. Am. Meteorol. Soc.*, *96*, 921–938, doi:10.1175/BAMS-D-13-00117.1.

Carton, J. A., and B. S. Giese (2008), A reanalysis of ocean climate using Simple Ocean Data Assimilation (SODA), *Mon. Weather Rev.*, *136*, 2999–3017.

Chang, P., L. Zhang, R. Saravanan, D. J. Vimont, J. C. H. Chiang, L. Ji, H. Seidal, and M. K. Tippett (2007), Pacific meridional mode and El Niño–Southern Oscillation, *Geophys. Res. Lett.*, *34*, L16608, doi:10.1029/2007GL030302.

Chen, D., et al. (2015), Strong influence of westerly wind bursts on ENSO diversity, *Nat. Geosci.*, *8*, 339–345, doi:10.1038/NGEO2399.

Chiang, J. C. H., and D. J. Vimont (2004), Analogous Pacific and Atlantic meridional modes of tropical atmosphere—Ocean variability, *J. Clim.*, *17*, 4143–4158.

Choi, J., S.-I. An, and S.-W. Yeh (2012), Decadal amplitude modulation of two types of ENSO and its relationship with the mean state, *Clim. Dyn.*, *38*, 2631–2644.

Deser, C., A. S. Phillips, R. A. Tomas, Y. Okumura, M. A. Alexander, A. Capotondi, J. D. Scott, Y.-O. Kwon, and M. Ohba (2012), ENSO and Pacific decadal variability in Community Climate System Model version 4, *J. Clim.*, *25*, 2622–2651.

Fedorov, A. V. (2002), The response of the coupled tropical ocean—Atmosphere to westerly wind bursts, *Q. J. R. Meteorol. Soc.*, *128*, 1–23.

Gierach, M. M., T. Lee, D. Turk, and M. J. McPhaden (2012), Biological response to the 1997–98 and 2009–10 El Niño events in the equatorial Pacific Ocean, *Geophys. Res. Lett.*, *39*, L10602, doi:10.1029/2012GL051103.

Kim, S. T., J.-Y. Yu, A. Kumar, and H. Wang (2012), Examination of the two types of ENSO in the NCEP CFS model and its extratropical associations, *Mon. Weather Rev.*, *140*, 1908–1923.

Kumar, K. K., B. Rajagopalan, M. Hoerling, G. Bates, and M. Cane (2006), Unraveling the mystery of Indian monsoon failure during El Niño, *Science*, *314*, 115–118.

Larson, S. M., and B. P. Kirtman (2014), The Pacific meridional mode as an ENSO precursor and predictor in the North American multimodel ensemble, *J. Clim.*, *27*, 7018–7032.

Lee, T., and M. J. McPhaden (2010), Increasing intensity of El Niño in the central-equatorial Pacific, *Geophys. Res. Lett.*, *37*, L14603, doi:10.1029/2010GL044007.

Linkin, M. E., and S. Nigam (2008), The North Pacific Oscillation–West Pacific teleconnection pattern: Mature-phase structure and winter impacts, *J. Clim.*, *21*, 1979–1997.

McPhaden, M. J. (1999), Climate oscillations—Genesis and evolution of the 1997–98 El Niño, *Science*, *238*, 950–954.

McPhaden, M. J., and X. Yu (1999), Equatorial waves and the 1997–98 El Niño, *Geophys. Res. Lett.*, *26*, 2961–2964, doi:10.1029/1999GL004901.

McPhaden, M. J., S. E. Zebiak, and M. H. Glantz (2006), ENSO as an intriguing concept in Earth Science, *Science*, *314*, 1740–1745.

McPhaden, M. J., T. Lee, and D. McClurg (2011), El Niño and its relationship to changing background conditions in the tropical Pacific, *Geophys. Res. Lett.*, *38*, L15709, doi:10.1029/2011GL048275.
Meinen, C. S., and M. J. McPhaden (2000), Observations of warm water volume changes in the equatorial Pacific and their relationship to El Niño and La Niña, *J. Clim.*, *13*, 3551–3559.
Mosquera-Vásquez, K., B. Dewitte, S. Illig, K. Takahashi, and G. Garric (2013), The 2002–2003 El Niño: Equatorial waves sequence and their impact on sea surface temperature, *J. Geophys. Res. Oceans*, *118*, 346–357.
Mosquera-Vásquez, K., B. Dewitte, and S. Illig (2014), The Central Pacific El Niño intraseasonal Kelvin wave, *J. Geophys. Res. Oceans*, *119*, 6605–6621, doi:10.1022/2014JC010044.
Newman, M., P. D. Sardeshmukh, and C. Penland (2009), How important is air-sea coupling in ENSO and MJO evolution, *J. Clim.*, *22*, 2958–2977.
Newman, M., S.-I. Shin, and M. A. Alexander (2011), Natural variation in ENSO flavors, *Geophys. Res. Lett.*, *38*, L14705, doi:10.1029/2011GL047658.
Ogata, T., S.-P. Xie, A. T. Wittenberg, and D.-Z. Sun (2013), Interdecadal amplitude modulation of El Niño–Southern Oscillation and its impacts on tropical Pacific decadal variability, *J. Clim.*, *26*, 7280–7297.
Penland, C., and P. D. Sardeshmukh (1995), The optimal growth of tropical sea surface temperature anomalies, *J. Clim.*, *8*, 1999–2024.
Rasmusson, E. M., and T. H. Carpenter (1982), Variations in tropical sea-surface temperature and surface wind fields associated with the Southern-Oscillation El Niño, *Mon. Weather Rev.*, *110*, 354–384.
Rodgers, K. B., P. Friederichs, and M. Latif (2004), Tropical Pacific decadal variability and its relation to decadal modulations of ENSO, *J. Clim.*, *17*, 3761–3774.
Rogers, J. C. (1981), The North Pacific Oscillation, *J. Climatol.*, *1*, 39–52.
Takahashi, K., A. Montecinos, K. Goubanova, and B. Dewitte (2011), ENSO regimes: Reinterpreting the canonical and Modoki El Niño, *Geophys. Res. Lett.*, *38*, L10704, doi:10.1029/2011GL047364.
Vimont, D. J., D. S. Battisti, and A. C. Hirst (2001), Footprinting: A seasonal link between the mid-latitudes and tropics, *Geophys. Res. Lett.*, *28*, 3923–3926, doi:10.1029/2001GL013435.
Vimont, D. J., J. M. Wallace, and D. S. Battisti (2003), The seasonal footprinting mechanism in the Pacific: Implications for ENSO, *J. Clim.*, *16*, 2668–2675.
Vimont, D. J., M. A. Alexander, and M. Newman (2014), Optimal growth of central and East Pacific ENSO events, *Geophys. Res. Lett.*, *41*, 4027–4034, doi:10.1002/2014GL059997.
Wang, S.-Y., M. L'Heureux, and H.-H. Chia (2012), ENSO prediction one year in advance using western North Pacific sea surface temperatures, *Geophys. Res. Lett.*, *39*, L05702, doi:10.1029/2012GL050909.
Wang, W., and H. H. Hendon (2007), Sensitivity of Australian rainfall to inter-El Niño variations, *J. Clim.*, *20*, 4211–4226.
Wittenberg, A. T. (2009), Are historical records sufficient to constrain ENSO simulations?, *Geophys. Res. Lett.*, *36*, L12702, doi:10.1029/2009GL038710.
Xie, S.-P. (1999), A dynamic ocean-atmosphere model of the tropical Atlantic decadal variability, *J. Clim.*, *12*, 64–70.
Yu, J.-Y., and S. T. Kim (2011), Relationships between extra-tropical sea level pressure variations, and the central-Pacific and eastern-Pacific types of ENSO, *J. Clim.*, *24*, 708–720.
Yu, J.-Y., H.-Y. Kao, and T. Lee (2010), Subtropics-related interannual sea surface temperature variability in the equatorial central Pacific, *J. Clim.*, *23*, 2869–2884.
Zhang, H., A. Clement, and P. Di Nezio (2014), The south Pacific meridional mode: A mechanism for ENSO-like variability, *J. Clim.*, *27*, 769–783.